The invariant algorithm for identification and detection of multiple gas plumes and weak releases.

Erin M. O'Donnell, David W. Messinger, Carl Salvaggio, and John R. Schott

Digital Imaging and Remote Sensing Laboratory
Chester F. Carlson Center for Imaging Science
Rochester Institute of Technology, 54 Lomb Memorial Drive, Rochester, NY

ABSTRACT

The ability to detect and identify gaseous effluents is a problem that has been pursued with limited success. It has been shown to be possible using the Invariant algorithm on synthetic hyperspectral scenes with a strong single gas release. That however, is a very specific case and leaves room for further investigation. This study looks at more realistic detection and release scenarios. Our implementation of the Invariant algorithm uses Singular Value Decomposition (SVD) to select basis vectors from a subspace of target gases in conjunction with a Generalized Likelihood Ratio Test (GLRT) to determine on a pixel by pixel basis how "like" the target gas each pixel is. The target gases are modeled in the image radiance space including atmospheric effects. Target spectra are modeled in both emission and absorption. This study investigates how well weak plumes are detected. Also, there will be a test of a mixed gas in a strong plume release. Finally, a situation where a weak multiple gas release will be discussed. Synthetic hyperspectral imagery in the long wave infrared region (LWIR) of the electromagnetic spectrum will be the predominate data used in this study. This algorithm has been found to be applicable for these detection and identification scenarios.

Keywords: gaseous effluents, invariant algorithms, hyperspectral imagery, plumes, target detection

1. INTRODUCTION

Detection and identification of gaseous effluents is in the forefront of homeland security. It has been shown that the invariant algorithm using the Maximum Distance Method (MaxD)[1] to select basis vectors can detect a strong single gas release.[2] This work will take this a step further and look at how the invariant method using Singular Value Decomposition (SVD), to select basis vectors, detects gases in realistic release situations. This study utilizes modeled hyperspectral imagery of weak plumes in the infrared region of the electromagnetic spectrum and considers some gases determined by the United States Environmental Protection Agency's Clean Air Act to be of concern.

Lisowski and Cook (1996) assessed the use of short wave infrared (SWIR) and midwave infrared (MWIR) hyperspectral imagery collected from the ground to identify SO_2 being emitted from a coal burning power plant. The results showed that SVD was able determine the extent of the SO_2 plume.

Healey and Slater (1999) developed the Invariant Algorithm for target detection under variable illumination and atmospheric conditions in hyperspectral imagery in the visible (VIS) and near infrared region (NIR) of the electromagnetic spectrum. The thrust of the algorithm is that the target is modeled under various viewing conditions and then compared to the test pixel in the image radiance space. In the sub-pixel implementation of the Invariant Algorithm as discussed by Thai and Healey (2002), not only is the target modeled but the background is modeled as well. The test pixel is considered to be either like the target or the background.

This study applies the sub-pixel version of the Invariant Algorithm to MWIR and LWIR hyperspectral imagery. In this case the targets will be gas absorption spectra; these target spectra will be modeled varying

Further author information: (Send correspondence to E. O'Donnell)
E. O'Donnell: E-mail: emo1683@rit.edu

Algorithms and Technologies for Multispectral, Hyperspectral, and Ultraspectral Imagery XI, edited by Sylvia S. Shen, Paul E. Lewis, Proceedings of SPIE Vol. 5806 (SPIE, Bellingham, WA, 2005) · 0277-786X/05/$15 · doi: 10.1117/12.603940

temperature and concentration rather than viewing conditions.

This paper discusses the Invariant Algorithm and how it will be implemented for this research. Then it will describe the target space and the radiance model that generated it. Next, there will be a discussion of the synthetic image generator DIRSIG[6] and the test imagery used in this study. Finally, the results will be presented and the paper will finish with the conclusions and future directions for this work.

2. INVARIANT METHOD

Target detection is usually done by converting a scene into a space where it would look most like the target. For example, in the reflective spectral region the atmosphere is compensated for in a test image because this reflectance space most resembles the conditions where the target spectrum was observed. This would allow for a higher target detection probability. However, in doing gas detections the target is transparent and in compensating for the atmosphere there is a chance that the target signature is being altered. So the traditional method is not optimal for gases. The invariant method the models the target in the various ways that it would be seen in the image space. For example in this study, the atmosphere is added to the target, and the gas concentrations and temperatures are varied creating a library of radiance vectors. The idea behind the invariant method is that all target variations in a dataset can be encompassed by defining a reduced set of basis vectors, linear combinations of which will recreate the original dataset. The library can be reduced by several means; SVD, MaxD, principal components, etc. The test scene will be evaluated using the Generalized Likelihood Ratio Test (GLRT). The GLRT will use basis vector sets to determine whether each pixel is more like the background or the target gas. Basis vectors are generated from the library of modeled target spectra using SVD. SVD will also be used on a section of the test image to create basis vectors of the background. A test pixel is evaluated using these basis vectors and the GLRT.

The absorption spectra used in this study were taken from the Pacific Northwest National Laboratory (PNNL)[7] database of gas absorption features. The radiance model used to describe the target space is,

$$L(\lambda) = [\epsilon_s(\lambda)B(\lambda, T_s)\tau_p(\lambda) + \epsilon_p(\lambda)B(\lambda, T_p)]\tau_a(\lambda) + L_u(\lambda), \tag{1}$$

where $L(\lambda)$ is the total radiance. The Planckian radiance at the temperature of the surface, $B(\lambda, T_s)$, is attenuated by the emissivity of the surface, $\epsilon_s(\lambda)$ and the transmission of the plume, $\tau_p(\lambda)$. This is added to the Planckian radiance of the gas, $B(\lambda, T_p)$, at the plume temperature, T_p, attenuated by the emissivity of the plume, $\epsilon_p(\lambda)$. This is then all multiplied by the transmission of the atmosphere, $\tau_a(\lambda)$, and finally, the upwelled radiance, $L_u(\lambda)$ is added in. Assuming the plume is optically thin and using Kirkoff's Law the plume is further described by the transmission of the plume which, is written as

$$\tau_p(\lambda) = 1 - \epsilon_p(\lambda) \approx 1 - ck(\lambda, T_g). \tag{2}$$

The concentration path length of the gas is c, and the absorption spectrum of the gas is $k(\lambda, T)$ at a particular temperature as measured in the lab. The PNNL database contains several gases at three different temperatures, T_g, (5^oC, 25^oC, 50^oC). The concentration and temperature ranges for the target subspace were generated for gas spectra between 1-1000 ppm-m and $\pm 15^oC$ from the mean scene derived brightness temperature, respectively. The variability in the target space comes from this range of parameters; not from the atmosphere. The contrast between the surface temperature, which was held at 36^oC, and the plume temperature allows for the study to evaluate gas target spectra in emission and absorption. The values for $\tau_a(\lambda)$ and the $L_u(\lambda)$ were generated by a MODTRAN mid-latitude summer atmosphere and are the same for each gas library. The background is assumed to contain mostly high emissivities which result in low reflective values so a downwelled term is disregarded.

The algorithm is invoked iteratively for each gas. Several target spaces are generated, one for each gas species. The images are tested for each gas independent of the other gases. No "mixed gas" target spectra are created. This is how model generates the target gases and doesn't consider gas mixtures.

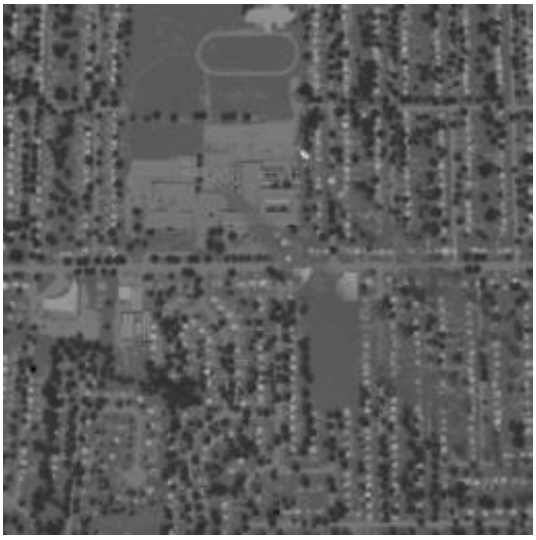

Figure 1. A single band of a test DIRSIG scene[6] prior to processing at $10.73\mu m$. There are two plumes in the scene.

3. TEST DATA SET

The test imagery used in this study were generated by DIRSIG,[8] a physics based synthetic image generator developed by the Digital Imaging and Remote Sensing Group at the Rochester Institute of Technology. This system allows for truth maps to be output with the test imagery. This allows the user to know exactly where the plume is and the temperature and concentration of the gas species, etc., in every pixel in the image. The spectra for materials used in the scene were obtained from either laboratory or field collects in addition to the target gases that were discussed previously. The $10.73\mu m$ band of a test scene is shown in Figure 1. This implementation of DIRSIG uses a sensor model similar to that of the SEBASS[9] instrument. The modeled scene uses only the longwave infrared (LWIR) channels instead of the full sensor implementation in both the MWIR and LWIR. The noise added to the modeled system mimics that of the SEBASS sensor and is spectrally correlated. The plume model used in DIRSIG is that of the Jet Propulsion Lab (JPL) plume model[10] which implements a Gaussian concentration and temperature distribution orthogonal to the downwind direction and exponential distribution downwind. This results in a full three dimensional model of a plume. The DIRSIG rendering of the JPL model is considered to be spectrally accurate although the spatial fidelity is low. For more information on DIRSIG and the plume model refer to Schott, *et al.* (1999) and Kuo (2000) respectively.

The background basis vectors input to the GLRT were derived from running SVD against a DIRSIG scene that was generated without the plumes implemented. When using real imagery a region of interest within the scene in an area where there was assumed to be no plume should be used in order to obtain background basis vectors.

4. RESULTS

The GLRT outputs the likelihood of finding the test gas in each pixel. The algorithm was run such that for each gas a result map was output as a "band" of an image cube. Table 1 describes how an image cube was laid out.

In the first test scene there were two weak plumes, each having a single gas release; freon-114 and ammonia. Regions of interest (ROI's) were created, as shown in Figure 2, over which the mean detection response was computed for each gas in the target set (see Figures 3 and 4). Here a weak plume consists of each gas being released at 0.25 g/s. The concentration path length of the gas over the ROI ranges from tens of ppm-m to tenths of a ppm-m. The output images, for freon and ammonia, from the GLRT are shown in Figures 5 and 6. The freon-114 plume results in a very dramatic detection map, Figure 5. Figure 3 shows that the average

Table 1. The list of gases as they correspond to the bands of the output GLRT hyperspectral image cube.

Band Index	Gas	Band Index	Gas
1	Acrolien	15	Freon-125
2	Fluorobenzene	16	Freon-12
3	Benzene	17	Freon-134a
4	Carbon tetrachloride	18	Freon-218
5	Methyl chloride	19	Formaldehyde
6	Methane	20	Hydrogen chloride
7	Carbon dioxide	21	Ammonia
8	Carbon monoxide	22	Phosgene
9	Dichloromethane	23	Sulfur hexafloride
10	1,2-Dichloropropane	24	Sulfur dioxide
11	1,3-Dichloropropane	25	1,1,2,2-Tetrachloroethane
12	1,2-Dibromomethane	26	Tetrachloroethane
13	1,2-Dichloromethane	27	Vinyl chloride
14	Freon-114		

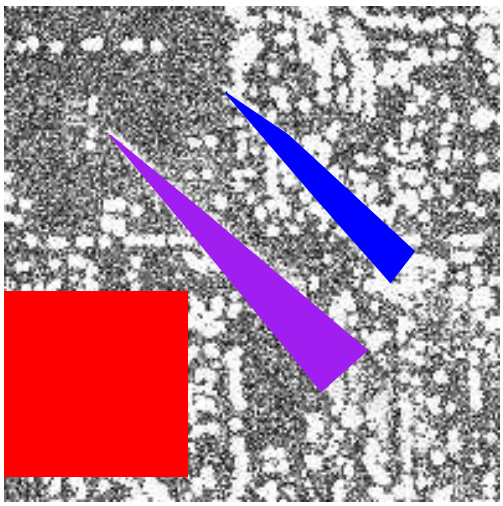

Figure 2. An output band of the GLRT; ROI's are shown for both plumes and a region of the background.

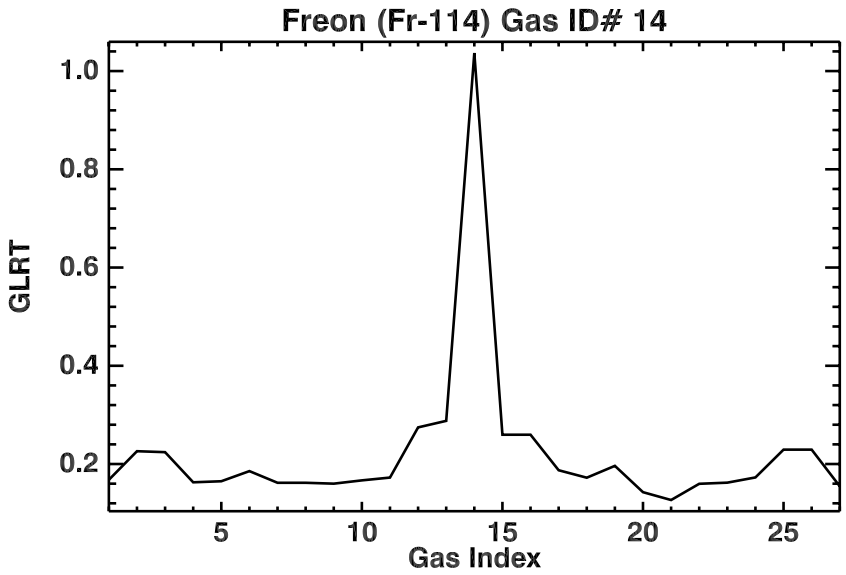

Figure 3. The output average plume spectra showing a high return in the freon band.

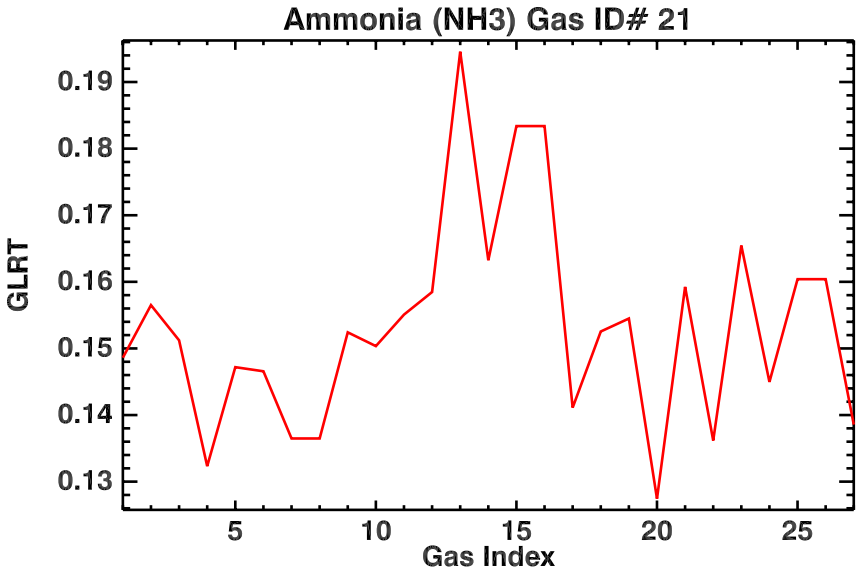

Figure 4. The output average plume spectra of the ammonia release.

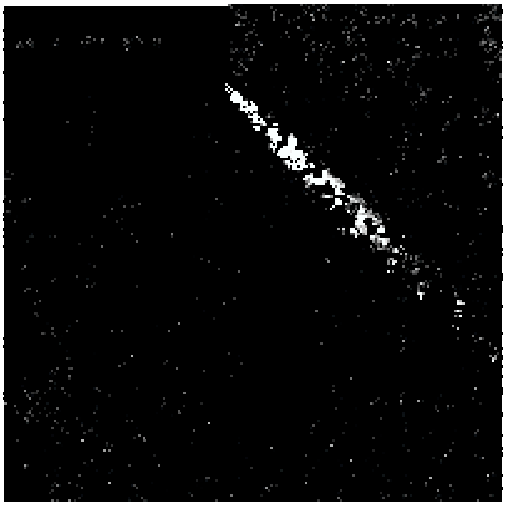

Figure 5. The freon band of the output GLRT image cube.

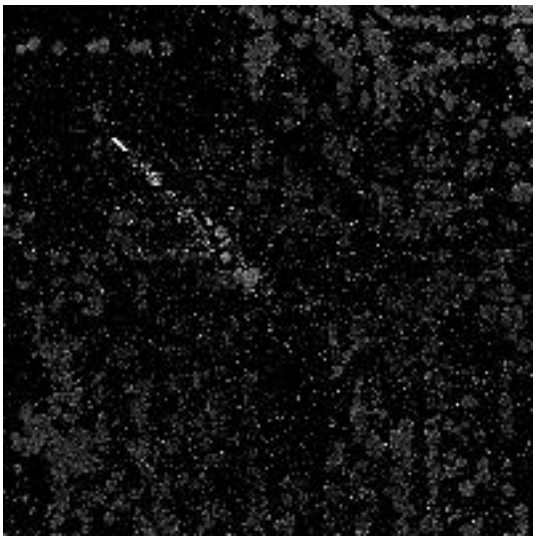

Figure 6. The output ammonia band from the GLRT image cube.

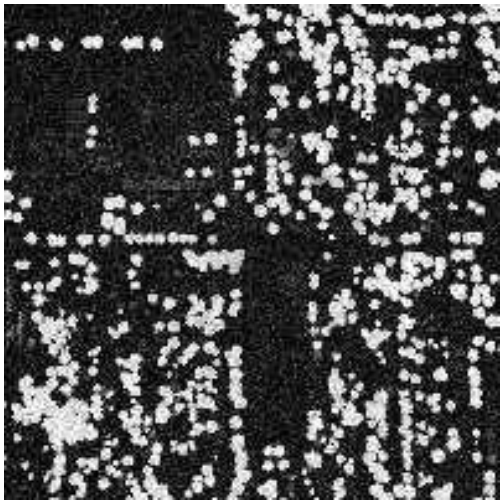

Figure 7. The gas index number 13 detection map showing null results for the ammonia plume.

detection of freon in the plume region is much greater in the freon band than in any of the other gas bands. The ammonia plume does not have such a strong contrast in the detection map, Figure 6 and although the results of averaging the return from the ROI of the ammonia plume, Figure 4, seem poor, the detection map still shows the plume structure. Figure 7 shows the detection map for the band having the highest return in the ammonia plume region. Despite its high value this does not correspond to a significant structure within the detection map; this meaning the plume does not show in the detection map. It is also notable to show that the freon-114 (gas index 14) return over the region of the ammonia plume is higher than the ammonia band and Figure 5 does not show the ammonia plume.

The next test scene was a mixed gas case with a "strong" release (50 g/s); one plume with two gases in it: freon-114 and 1,1,2,2-tetrachloroethane. Figure 8 shows that freon-114 gives the strongest return of all the gases in the plume region (gas index 14). This is further confirmed by Figure 9. The second highest detection is not the other gas in the plume,1,1,2,2-tetrachloroethane (gas index 25). However, looking at the detection result for 1,1,2,2-tetrachloroethane there is a distinguishable plume in the detection map, Figure 10. The gas 1,1,2,2-tetrachloroethane is a hard gas to detect because its strongest features are reduced due to the sensor response and atmospheric effects. This can be seen when comparing the lab spectra in, Figure 11, and the modeled target spectra, Figure 12, which have incorporated atmospheric effects and have been interpolated to a SEBASS-like spectral response. The modeled spectrum for freon-114 still has some strong features, which are right in the sensor range. The strongest features of 1,1,2,2-tetrachloroethane are centered around 13 μm and are barely noticeable in the modeled spectra.

Finally, the last test case is a weak multiple gas release of ammonia and 1,1,2,2-tetrachloroethane. The results from this are shown in Figure 13. Unfortunately the averaged plume region does not show a significant return for the target gases, however, as shown previously this does not necessarily mean that the algorithm fails. There should be strong returns in "bands" 21 and 25. The detection maps for these bands are shown in Figures 14 and 15 respectively. While the ammonia in the plume is distinguishable there is not a significant detection of 1,1,2,2-tetrachloroethane in the detection map. However, after further investigation of the other gas detection

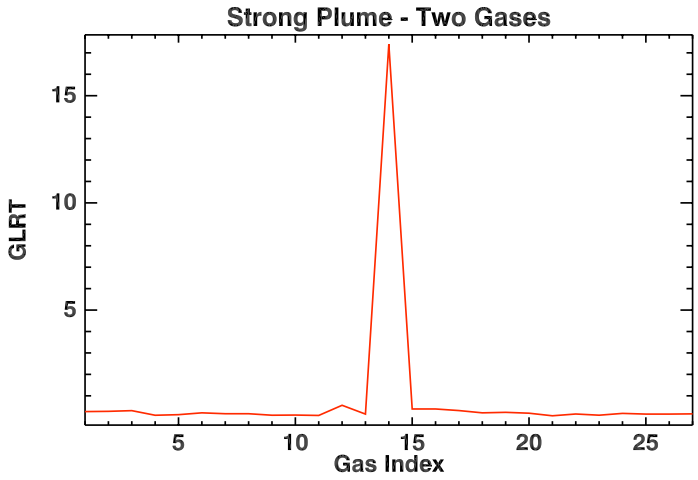

Figure 8. The GLRT results for the mixed gas in a strong release; showing a significant return for freon-114.

Figure 9. The freon-114 detection map for the mixed gas in a strong release.

Figure 10. The 1,1,2,2-tetrachloroethane detection map for the mixed gas in a strong release.

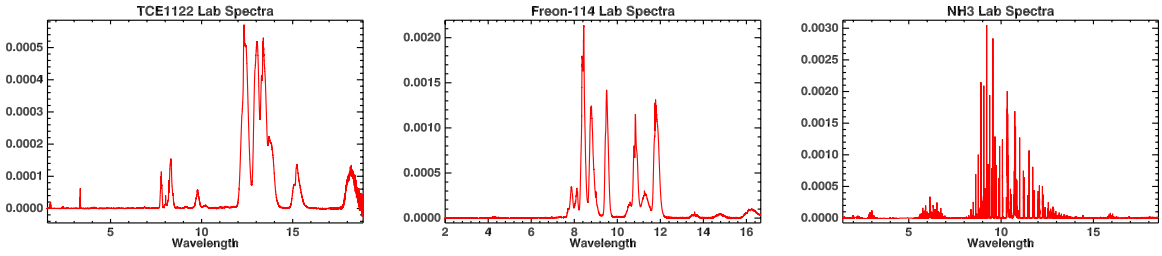

Figure 11. PNNL lab spectra for (a) 1,1,2,2-Tetrachloroethane (b)Freon-114 (c) Ammonia (NH_3)

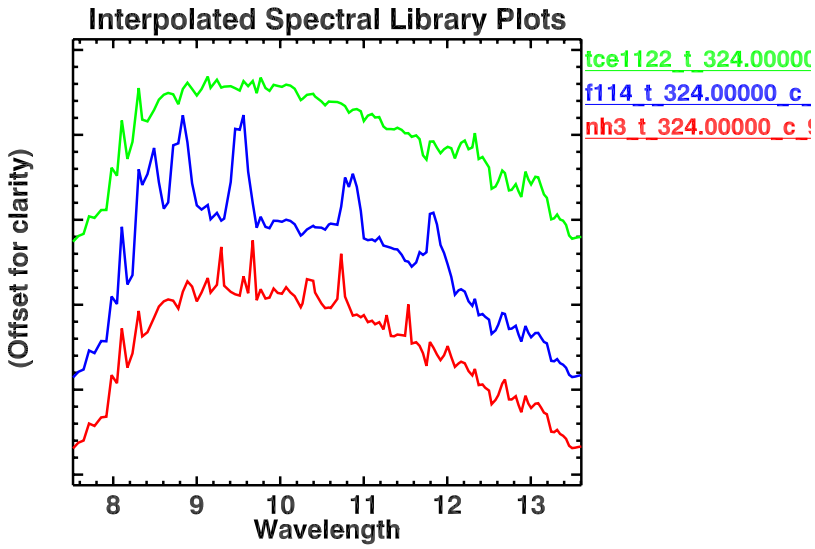

Figure 12. Example modeled target spectra (from top to bottom: 1,1,2,2-tetrachloroethane, freon-114 and ammonia).

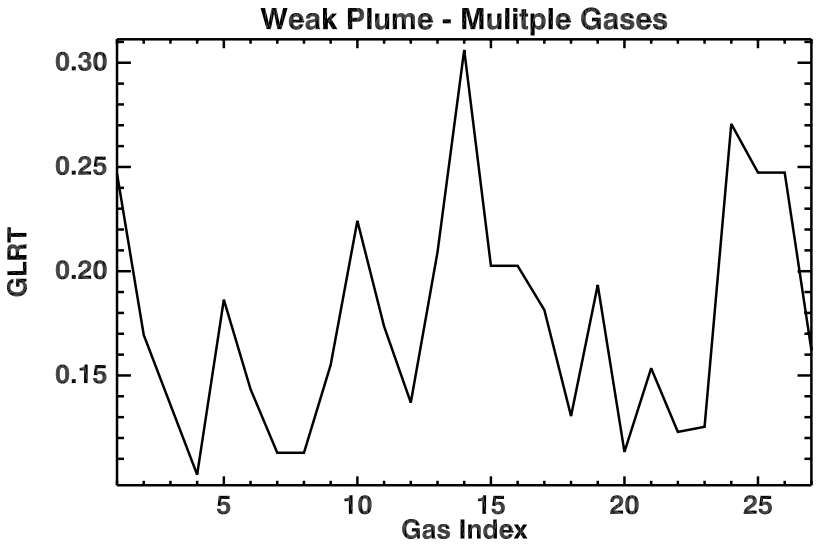

Figure 13. The GLRT output for a mixed gas weak release.

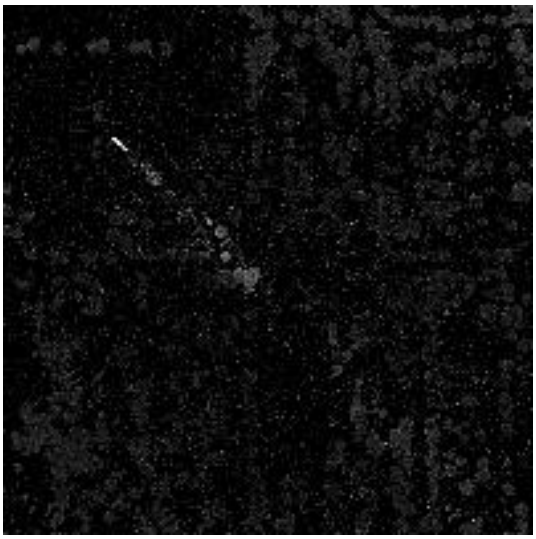

Figure 14. The detection map for ammonia in a mixed gas weak release.

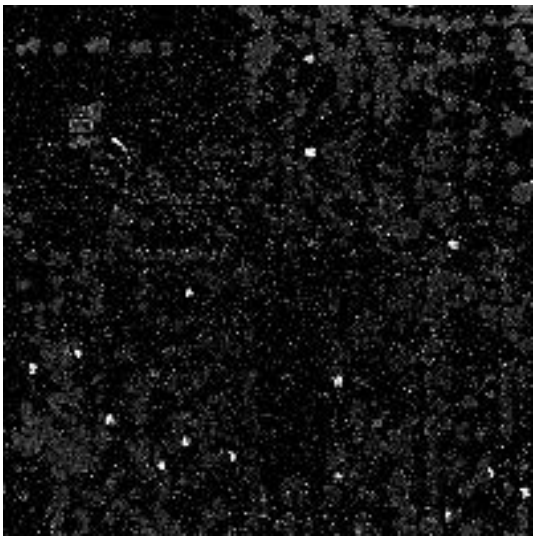

Figure 15. The detection map for 1,1,2,2-tetrachloroethane in the mixed gas weak release.

bands the plume structure in these images is significant. Also, it is notable that there are maximum returns from pixels near to the stack for both target gases.

5. CONCLUSION AND FUTURE WORK

The results for weak plumes and mixed plumes are promising. Normalization of the detection images would improve the spectral detection results per gas in the image cube. When investigating weak plumes smaller ROI's should be used. This would be more applicable if the algorithm is failing at the low temperatures and concentrations. This implies that the target model must incorporate lower temperatures and concentrations to achieve better detection downwind of weak plumes. Also, the overall detections could improve with a better selection of background basis vectors. As can be seen in the detection maps there are some patches that have better returns than others where the background material is obviously the culprit. The mixed gas cases are not giving as definitive results as would be desired. Not only would these cases benefit from a better description of the background but a better model for the target space. Currently the model is run such that each gas is considered independently. A target space generated for mixed gases would be more appropriate for detecting mixed gases.

ACKNOWLEDGMENTS

This research was funded under the Office of Naval Research Multi-disciplinary University Research Initiative "Model-based Hyperspectral Exploitation Algorithm Development", no. N00014-01-1-0867. Any opinions, findings, and conclusions or recommendations expressed in this material are those of the authors and do not necessarily reflect the views of the Office of Naval Research.

REFERENCES

1. P. Bajorski, E. Ientillucci, and J. Schott, "Comparison of basis-vector selection methods for target and background subspaces as applied to subpixel target detection," in *Algorithms and Technologies for Multispectral, Hyperspectral, and Ultraspectral Imagery X, Proceeding of SPIE, v. 5425*, 2004.
2. E. O'Donnell, D. Messinger, C. Salvaggio, and J. Schott, "Identification and detection of gaseous effluents from hyperspectral imagery using invariant algorithm," in *Algorithms and Technologies for Multispectral, Hyperspectral, and Ultraspectral Imagery X, Proceeding of SPIE, v. 5425*, 2004.
3. J. Lisowski and C. Cook, "A svd method for spectral decomposition and classification of ares data," *SPIE* **2821**(15), pp. 14–19, 1996.
4. G. Healey and D. Slater, "Models and methods for automated material identification in hyperspectral imagery acquired under unknown illumination and atmospheric conditions," *IEEE Trans. Geo. Rem. Sens.* **37**(6), pp. 2706–2717, 1999.
5. B. Thai and G. Healey, "Invariant subpixel material detection in hyperspectral imagery," *IEEE Trans. Geo. Rem. Sens.* **40**(3), pp. 599–608, 2002.
6. E. Ientilucci and S. Brown, "Advances in wide area hyperspectral image simulation," in *Conference on Targets & Backgrounds IX: Characterization and Representation, Proceedings of SPIE, v. 5075*, pp. 110–121, 2003.
7. S. Sharp *et al.*, "Creation of 0.10 cm^{-1} resolution, quantitative, infrared spectral libraries for gas samples," in *Vibrational Spectroscopy-Based Sensor Systems, Proceedings of SPIE, v. 4577*, S. Christesen and A.J. Sedlacek, III, eds., pp. 12–24, 2001.
8. J. Schott, S. Brown, R. Raqueño, H. Gross, and G. Robinson, "An advanced synthetic image generation model and its application to multi/hyperspectral algorithm development," *Can. J. Rem. Sen.* **25**(2), pp. 99–111, 1999.
9. J. Hackwell, D. Warren, R. Bongiovi, H. S.J., T. Hayhurst, D. Mabry, M. Sivjee, and J. Skinner, "Lwir/mwir imaging hyperspectral sensor for airborne and ground-based remote sensing," in *Imaging Spectrometry II, Proceedings of SPIE, v. 2819*, M. Descour and J. Mooney, eds., pp. 102 – 107, 1996.
10. J. Halitsky, "A jet plume model for short stacks," *JAPCA Note-Book* **39**(6), pp. 856–858, 1989.
11. S. Kuo, J. Schott, and C. Chang, "Synthetic image generation of chemical plumes for hyperspectral applications," *Opt. Eng.* **39**(4), pp. 1047–1056, 2000.